Comparison of 3D TLM Meshing Techniques for Modeling Microwave Components

J. L. Herring and W. J. R. Hoefer

NSERC/MPR Teltech Research Chair in RF Engineering,
Department of Electrical & Computer Engineering, University of Victoria,
P. O. Box 3055, Victoria, B. C., V8W 3P6, Canada.

Abstract

The application of graded mesh and multigrid techniques to the modeling of microwave components in 3-dimensions with the TLM method are discussed. Comparisons are made for graded mesh and multigrid interfaces in a waveguide, for a non-touching axial strip placed in a waveguide, and for a microstrip impedance step. The issues of appropriate excitation and absorbing boundary conditions are addressed. It is shown that multigrid techniques provide an effective means of reducing the mesh resolution away from discontinuities.

Introduction

The transmission-line matrix (TLM) method of numerical electromagnetic analysis with the symmetrical condensed node (SCN) [1] is well established. To increase the flexibility in which a problem can be meshed, two main techniques have been proposed: graded mesh and multigrid mesh. In this paper, graded and multigrid techniques will be applied to simple waveguide and microstrip examples, and the relative efficiency and accuracy will be compared.

Graded Mesh

A graded mesh is defined by the cell dimensions along each of the coordinate axes. A feature of graded meshes is that fine mesh regions cannot be completely isolated from the rest of the mesh. In the original approach, the link-line impedances were kept constant and stubs were added at the nodes (the *stub-loaded* node). However, if the nodes are far from being cubic, this imposes an unreasonable limit on the timestep. The *hybrid* node [2] offers a more favorable limit on the timestep and also has superior dispersion characteristics.

Multigrid Schemes

Multigrid techniques allow connection between two disjoint meshes. These meshes can be uniform (with cubic or cuboid nodes) or they can be graded. At least three multigrid schemes have been proposed and these will be referred to as methods *A*, *B* and *C* in this paper.

In method *A*, the average field is maintained across the fine/coarse mesh interface (this is equivalent to conserving charge) and the coarse→fine and fine→coarse conversions are dealt with separately [3]. The coarse and fine mesh timesteps can be equal but it is more useful to run the fine mesh with a smaller timestep. For example, if both meshes are uniform and cubic, the standard 12-port node can be used for both meshes and each mesh can be run with the maximum timestep of $\Delta l/2c$. In situations where the fine and coarse mesh timesteps are not equal, it is essential that the calculation is ordered such that an axial TEM wave will propagate perfectly. The standard 12-port node is the most efficient SCN formulation and it is also the most accurate for axial propagation. If a node is used in which the link-line impedance can vary over the interface, then appropriate reflection and transmission coefficients may need to be applied before the conversion takes place [4]. For the hybrid node, this must be done if the ratio of the timestep and the normal node dimension are not the same in both the fine and coarse meshes. The main disadvantage of method *A* is that there is a loss of energy in the fine→coarse conversion.

In method *B*, the fine/coarse mesh interface is implemented as an electrical connection [5]. Energy is conserved in the conversion procedure but it does require that both fine and coarse meshes are run with the same timestep. This means that the standard 12-port node cannot be used for the coarse mesh (e.g. stub-loaded or hybrid nodes must be used), resulting in longer run-times and a higher memory requirement. The fine→coarse conversion is identical to that in method *A*. For the coarse→fine conversion, for the case when the incident fine mesh pulses are not equal, the extra degrees of freedom needed

to enforce both charge and energy conservation, are accommodated by modifying the reflected fine mesh pulses. There is a choice in whether to connect the fine mesh link-lines by row first or by column first, although in practice there appears to be little difference between the two.

In method *C*, the interface is implemented by fitting a two-dimensional spline to the pulses incident upon the interface and then calculating the transmitted pulses by interpolation [6]. This method allows greater flexibility in both spatial and temporal discretization, for example, a non-integer number of link-lines from the fine mesh can be connected to a non-integer number of link-lines from the coarse mesh. However, the procedure does not enforce conservation of energy and, in contrast to method *A*, there can be a gain of energy, as well as a loss. There is also the problem of trying to fit a spline in the presence of spurious modes with a high spatial frequency. Such modes can be predicted theoretically [7] and, in practice, are often observed close to excitation points. Spurious modes do not present a problem to methods *A* and *B*, and since these methods usually provide adequate options for meshing, they will be concentrated on in this paper.

Meshing Methodology

Both graded mesh and multigrid methods have been used as mesh refinement techniques, so that a uniform fine mesh does not have to be used throughout the entire problem space. However, for certain discontinuities, mesh refinement may not give a significant improvement. Normally, TLM is expected to be second order accurate but in the presence of, for example, a knife-edge discontinuity, the accuracy is reduced to first order [8,9]. When such discontinuities are present, the only practical solution is to make use of local mesh modification techniques. These techniques can be based on analytical formulations [10], or on correction factors obtained from an optimization procedure [11]. Special nodes are also available for wires and slots [12,13], where the features are much smaller than the cell size.

Mesh grading can be used to fit the mesh to the exact physical dimensions of the structure under study. However, since the cell dimensions must be constant along each of the axes, this means that unless the features of the structure are aligned, then small cells must be introduced. This will have a detrimental affect on the timestep. Alternatively, the size of cells adjacent to short or open-circuit boundaries can be varied continuously by altering the link-line impedance [14]. For the SCN, the arm length can be reduced to one half of the standard value (the presence of the side arms means that the length cannot be reduced below this), or the length can be increased arbitrarily. This procedure works well for normal incidence.

The most appropriate use of multigrid techniques is to reduce the resolution away from discontinuities. For example, by increasing the distance to absorbing boundary conditions (ABC's), the effect of higher order modes is reduced and better absorption is obtained. Multigridding can also be used to connect disjoint graded meshes for structures with features which are not aligned.

Interface Between Two Meshes in a Waveguide

Following the example of *Wlodarczyk* [5], the accuracy of multigrid schemes can be assessed by calculating the S-parameters of the interface in a section of waveguide. The ends of the waveguides can be terminated with modal diakoptic boundaries [15,16]. For a uniform mesh, the reflection from these ABC's is close to the limit of numerical precision (-120dB single precision, -300dB double precision) and so they will not distort the results. There are no resonance elements present, so the simulation will be short and the discrete Green's function does not need to be truncated. To avoid problems with sampling the field at a single point in meshes of different resolution, a modal decomposition is performed over the cross-section to extract the mode amplitude.

Fig. 1 shows the reflection and transmission coefficients for multigrid interfaces between a 16x8 coarse mesh and a 32x16 fine mesh, for methods *A* and *B*. The nodes are cubic in all cases. Two cases are considered for method *B*: stub-loaded coarse mesh and hybrid node coarse mesh. The standard 12-port node is used for all other meshes. For method *B*, the reflection coefficients are the same for both coarse→fine and fine→coarse conversions. Also, the transmission coefficients are symmetrical about unity. Smaller reflections are obtained with the hybrid node coarse mesh. For method *A*, the fine→coarse conversion works better than the coarse→fine conversion. The reflection coefficient for the fine→coarse conversion is better than for method *B*. Both transmission coefficients are much less frequency dispersive, particularly the fine→coarse conversion. This means that if it is only the fine→coarse conversion which is of interest (e.g. the region of interest is contained in the fine mesh and the coarse mesh is only used to increase the distance to ABC's), method *A* can give superior results. However, if the system contains resonant elements, and if the oscillation occurs across the interface, then the loss of energy will be a problem and method *B* will be more appropriate.

The magnitudes of the reflection and transmission coefficients for a multigrid interface are similar to those observed with a straightforward graded mesh interface. Fig. 2 shows curves for an interface between cubic nodes and nodes with normal

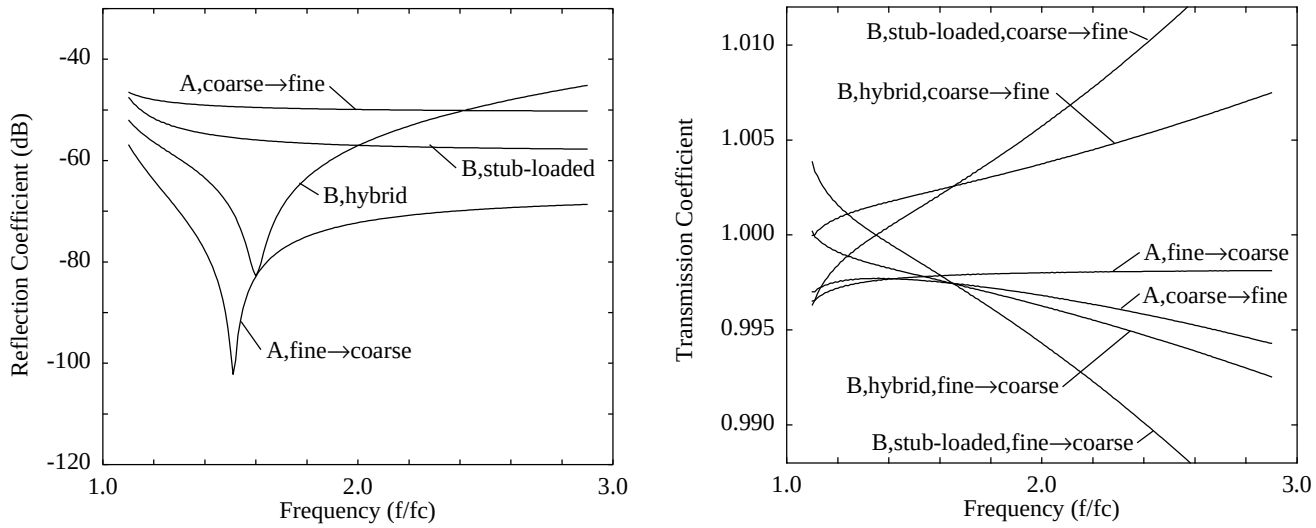

Fig. 1 – Reflection and transmission coefficients for multigrid interface between 16x8 coarse mesh and 32x16 fine mesh

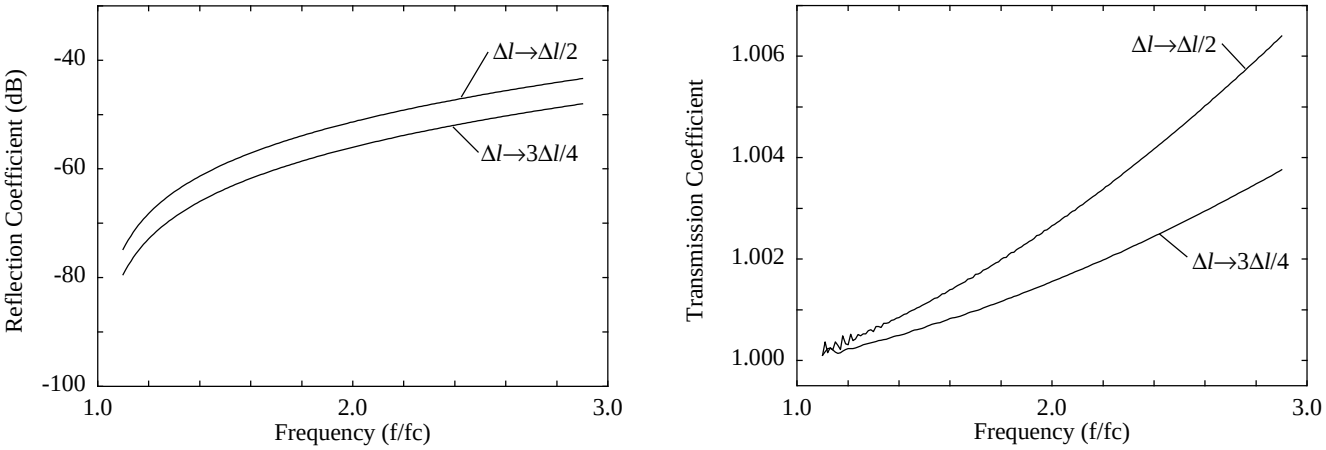

Fig. 2 – Reflection and transmission coefficients for hybrid node graded mesh, 16x8 node cross-section

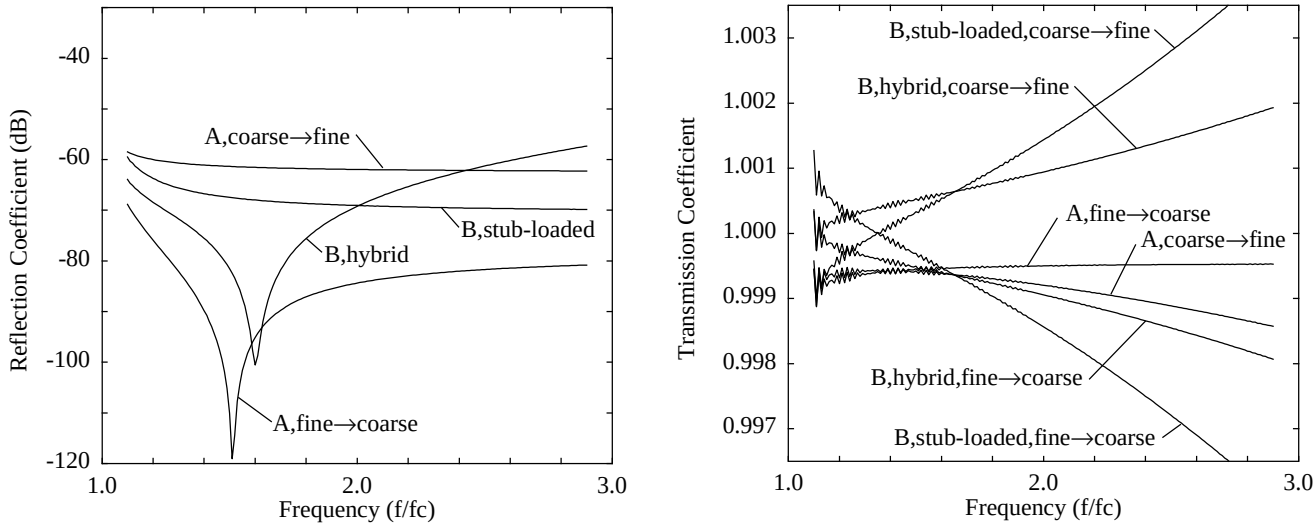

Fig. 3 – Reflection and transmission coefficients for multigrid interface between 32x16 coarse mesh and 64x32 fine mesh

dimensions of $\Delta l/2$ and $3\Delta l/4$, modeled with the hybrid node. The curves are functions only of the initial and final node dimensions; the same results are obtained if the node dimensions are changed in one step or if they are changed gradually.

The performance of multigrid interfaces improves as the mesh resolution is increased. Fig. 3 is the same as Fig. 1 except that both coarse and fine meshes are doubled in resolution. The trends observed are the same as in the previous case.

Non-touching Axial Strip in a Waveguide

A simple three-dimensional discontinuity consisting of a non-touching axial strip placed in a waveguide, as shown in Fig. 4, has been modeled. The dimensions of the strip are such that for Δl=0.1185mm, the strip is exactly 3x16 nodes and the waveguide cross-section is 60x30 nodes. Symmetry can be exploited about the strip. The size of this strip presents a challenge to the modeler: if the strip was very small compared to the mesh size, a special node (similar to a wire node) would have to be used; if the strip was much larger, then a straightforward TLM description would probably be sufficient. Here, an edge correction is applied around the strip to reduce the coarseness error [11]. The correction factors were obtained from a systematic optimization for a single finned waveguide, and if the correct result is obtained for this structure, it will give a measure of the generality of the method and of the correction factors.

To allow comparison between different meshing schemes, the strip is described in a uniform fine mesh 13 nodes in length, as shown in Fig. 5. The output planes are taken three nodes from the edge of the strip (the edge correction extends over nodes 5 and 9). Since the output planes are close to the strip, a modal decomposition must be performed over the cross-section to extract the dominant mode amplitude. This is done from the *Hz* field component. In the general case, where it is necessary to distinguish between TE and TM modes of the same order, it is more convenient to work with *Hz* and *Ez* rather than with the voltage pulses. This is in contrast to the usual implementation of modal diakoptic ABC's, which work directly on the voltage pulses [16]. For the excitation, *Ey* is introduced with the spatial distribution of the dominant mode, on the same plane as the first port output. Special care must be taken when calculating the field at the same point as the excitation since the usual condition, that the incident charge before scattering is the same as the reflected charge, does not hold. In this case, *Hz* must be calculated from both incident and reflected voltage pulses. The pulses needed to produce the required excitation waveform are obtained from a reference structure containing hard voltage sources [17]. This reference structure is only a single cell in length and is terminated with dominant mode diakoptic ABC's.

Given that the strip is adequately described in the fine mesh, the main decision to be made is on the waveguide terminations. Some of the available options are shown in Fig. 6. The waveguide can be terminated close to the strip, which requires an ABC that will adequately absorb higher order modes. The termination can be moved a short distance away, to reduce the number of modes to be absorbed, or, the termination can be moved far away, so that only the dominant mode needs to be considered. Single mode diakoptic ABC's and one-way equation ABC's [18] can be used in the last case. Multi-mode diakoptic ABC's can be used in the other cases, provided the modes are known in advance. The Berenger perfectly matched layer (PML) is also a possibility [19,20], although the PML must be of a certain thickness, which increases the computation effort. Multigridding provides an efficient way to distance ABC's by adding coarse mesh regions.

The results obtained with a uniform fine mesh (30x30x96 nodes) and dominant mode diakoptic ABC's are shown in Fig. 7, along with independent results [21,22]. There is very good agreement considering the small number of nodes describing the strip. The effect of adding a coarse mesh to the original 13 node fine mesh is shown in Fig. 8, for lengths of 20 and 5 coarse mesh nodes, and for no coarse mesh, again for dominant mode ABC's. The 20 node coarse mesh gives results almost identical to the uniform fine mesh but with much reduced computing resources. To provide good terminations with multi-mode ABC's, modes up to 5,4 must be considered with no coarse mesh, and modes up to 3,2 with a 5 node coarse mesh. Placing modal diakoptic boundaries in a coarse mesh has the advantage that the modal decomposition can be performed more efficiently because there are fewer nodes in the cross-section. In a practical simulation, the output planes could be placed on the waveguide terminations, where the dominant mode amplitudes can be obtained directly from the ABC's.

For the previous results, a band-limited (modulated Gaussian) excitation was used. An impulse excitation (still with the spatial distribution of the dominant mode) could also be used. The only disadvantage is that energy is introduced at the waveguide cutoff frequency, causing a ringing effect which does not decay. The magnitude of the dominant mode at the input port is shown for the two cases in Fig. 9. The extraction of frequency domain characteristics in the second case is more challenging since the required signal is much smaller than the ringing. One possibility is to apply a window function before taking the Fourier transform. The point illustrated here is that the simulation remains perfectly stable with an impulse excitation, for both multigrid methods tested (*A* and *B*) with modal diakoptic ABC's. In practice, it is better to avoid exciting the waveguide cutoff and impulse excitation must be avoided altogether when certain elements are present, e.g. one-way equation ABC's.

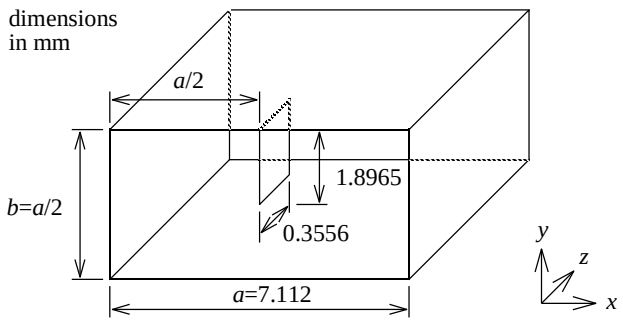

Fig. 4 – Geometry of non-touching axial strip

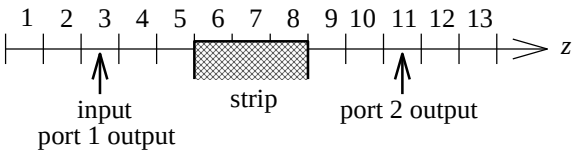

Fig. 5 – Discretization along the length of the waveguide

Fig. 6 – Meshing Schemes

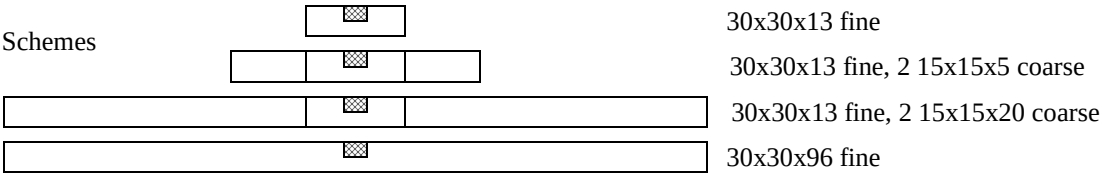

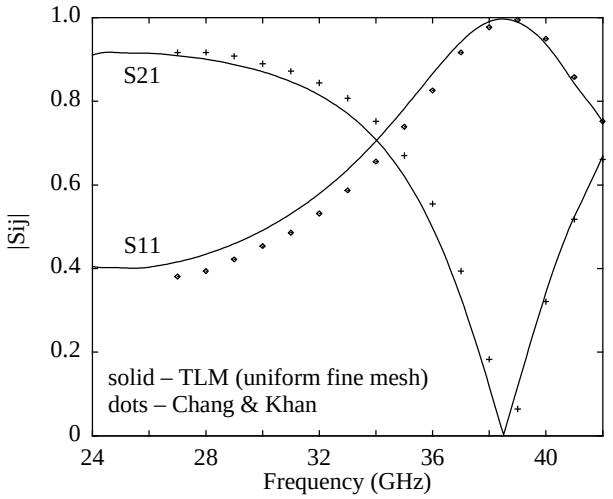

Fig. 7 – Non-touching strip: TLM and independent results

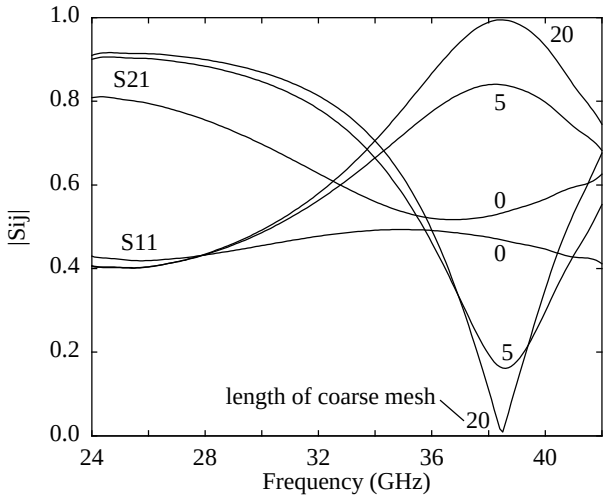

Fig. 8 – Non-touching strip: varying length of coarse mesh

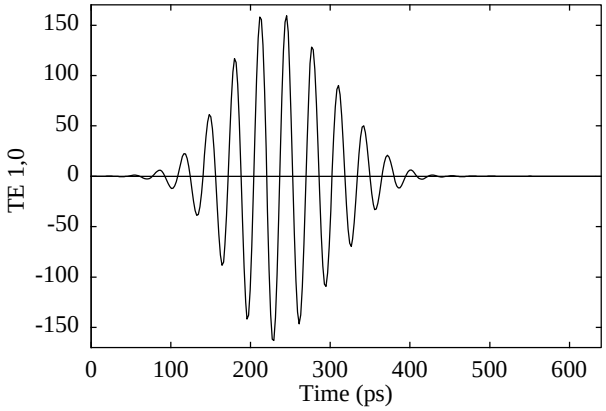

(*a*) band-limited (modulated Gaussian) excitation

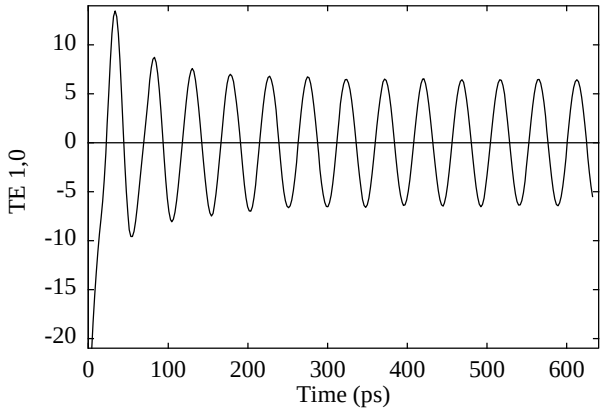

(*b*) impulse excitation

Fig. 9 – Non-touching strip: magnitude of the dominant mode taken from the total field at the input port

A comparison of the results obtained with different multigrid schemes is shown in Fig. 10. These curves show the difference (x0.001) between the multigrid results and the results from the long uniform fine mesh. The result from method *B* is much closer to the fine mesh result than method *A* and, interestingly, at higher frequencies, the stub-loaded coarse mesh is better than the hybrid node coarse mesh. However, the error introduced by any of these schemes is likely to be much less than the other errors involved.

A comparison of the run-times on a 100MHz HP 735 workstation is given below. 2000 fine mesh timesteps were performed in all cases. Runs marked with an asterisk gave poor results and are only included to give an indication of the computational effort. The best solution is to use multigridding to distance the ABC's. Method *A* runs in the shortest time but a slightly better result can be obtained with method *B*. Multi-mode ABC's are expensive compared to adding a coarse mesh region. It should be noted that these figures are very implementation dependant (for example, execution speed could be increased at the expense of an increase in storage requirement), so they should only be taken as a rough indication of the efficiencies of different meshing schemes.

Mesh	ABC	Run-time (sec.)
uniform fine 30x30x96	dominant mode diakoptics	1228
uniform fine 30x30x13	dominant mode diakoptics	422 *
uniform fine 30x30x13	multi-mode diakoptics, to order 3,2	886 *
uniform fine 30x30x13	multi-mode diakoptics, to order 5,4	1694
method A, 30x30x13 fine, 2 15x15x5 coarse	dominant mode diakoptics	430 *
method A, 30x30x13 fine, 2 15x15x5 coarse	multi-mode diakoptics, to order 3,2	514
method A, 30x30x13 fine, 2 15x15x20 coarse	dominant mode diakoptics	459
method B, 30x30x13 fine, 2 15x15x20 stub-loaded coarse	dominant mode diakoptics	582
method B, 30x30x13 fine, 2 15x15x20 hybrid coarse	dominant mode diakoptics	691

Microstrip Impedance Step

To accurately describe microstrips, a reasonable number of nodes must be taken across the width of the metallization and in the height of the substrate. A suitable ABC must be selected to terminate the microstrip. One-way equation ABC's can be used, in which the coefficients are based upon the effective dielectric constant of the microstrip [18]. In this example, simple matched boundaries (giving a reflection coefficient of zero) are used. Here, matched boundaries give adequate performance and some tuning of the coefficients would be required to get a superior performance from one-way equation ABC's. The side and top boundaries are also modeled with matched boundaries. These boundaries must be placed sufficiently far from the microstrip so that they do not disturb its operation. Adding a coarse mesh around the microstrip is an efficient method of increasing the distance to these boundaries. Excitation of microstrips must be done carefully. One possibility is to excite the vertical component of the E-field uniformly under the strip and to allow a certain distance for the correct field distribution to establish itself. Here, a complete plane is excited spatially with the d.c. E-field distribution and temporally with a Gaussian pulse. The d.c. field distribution is obtained from a 2-dimensional slice of TLM nodes, excited with a raised cosine voltage source placed between the ground plane and the strip. To encourage the decay of transients, all metallic surfaces are replaced with matched boundaries, since these will form an equipotential in the steady-state.

The example of an impedance step resulting from a 1:2 change in width is considered here. The dimensions, and details of the multigrid scheme are shown in Fig. 11. The results obtained from a uniform fine mesh with a cross-section of 72x48 nodes, and a mesh of 30x12 nodes (the same as that used in the multigrid schemes) are shown in Fig. 12. The S-parameters were calculated from the strip voltage, and to account for the different impedances of the input and output ports, a factor $\sqrt{Z_{01} \div Z_{02}}$ was included in the S21 calculation. The large fine mesh result agrees well with independent results [23]. The proximity of the ABC's in the small fine mesh causes a significant distortion to the results. Multigrid (method *A* and method *B* with both stub-loaded and hybrid nodes) and graded mesh (hybrid node) schemes are compared in Fig. 13. The graded mesh has the same cell dimensions in the cross-section as the multigrid schemes and the same longitudinal dimensions as the fine mesh. The result from the graded mesh is identical to the uniform fine mesh. The 51x30 uniform fine mesh actually gives slightly better agreement than multigrid method *A*. However, all multigrid schemes have half as many nodes in the longitudinal direction in the coarse mesh. Of the multigrid schemes, method *B* with the hybrid node gives the best agreement. It should be noted that there are still errors present in the simulation, in that the curves should be much flatter in the frequency range. In summary, the graded mesh gives the most accurate result but multigrid method *A* runs the fastest.

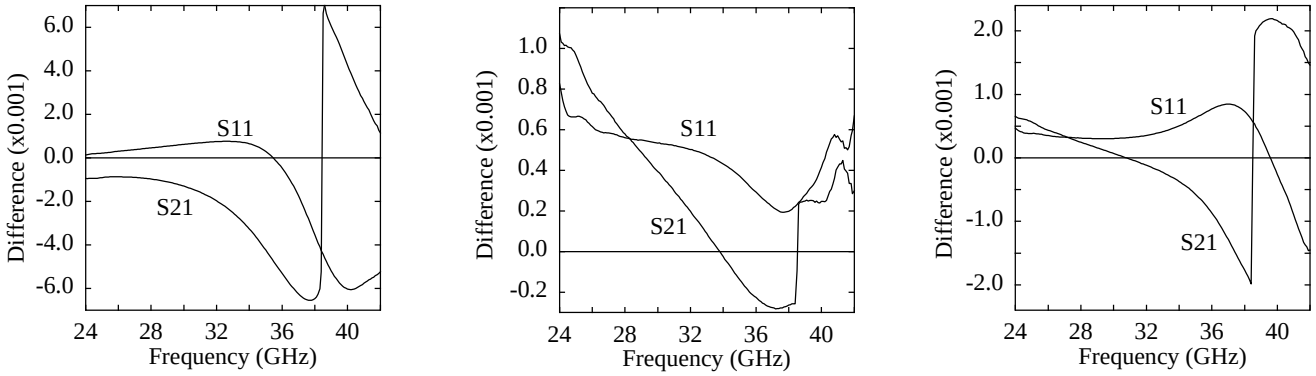

(*a*) method *A* (*b*) method *B*, stub-loaded node (*c*) method *B*, hybrid node

Fig. 10 – Non-touching strip: difference in S-parameters obtained with different multigrid schemes

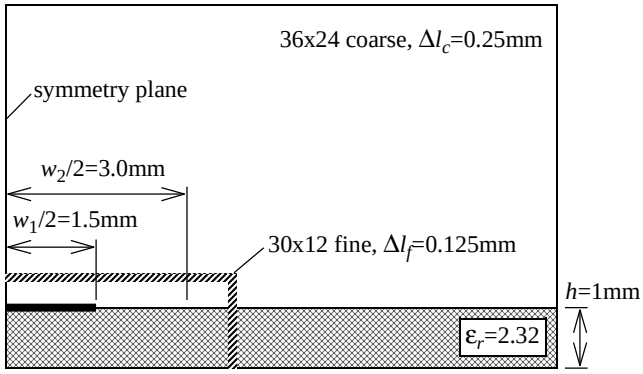

Fig. 11 – Multigrid mesh for microstrip impedance step

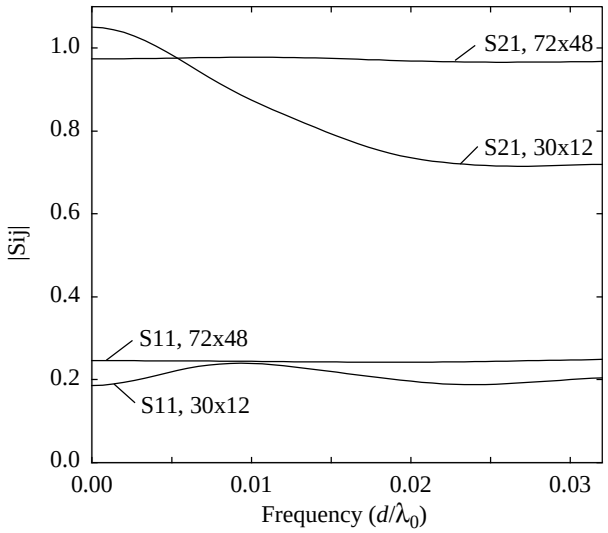

Fig. 12 – Impedance step: uniform fine mesh

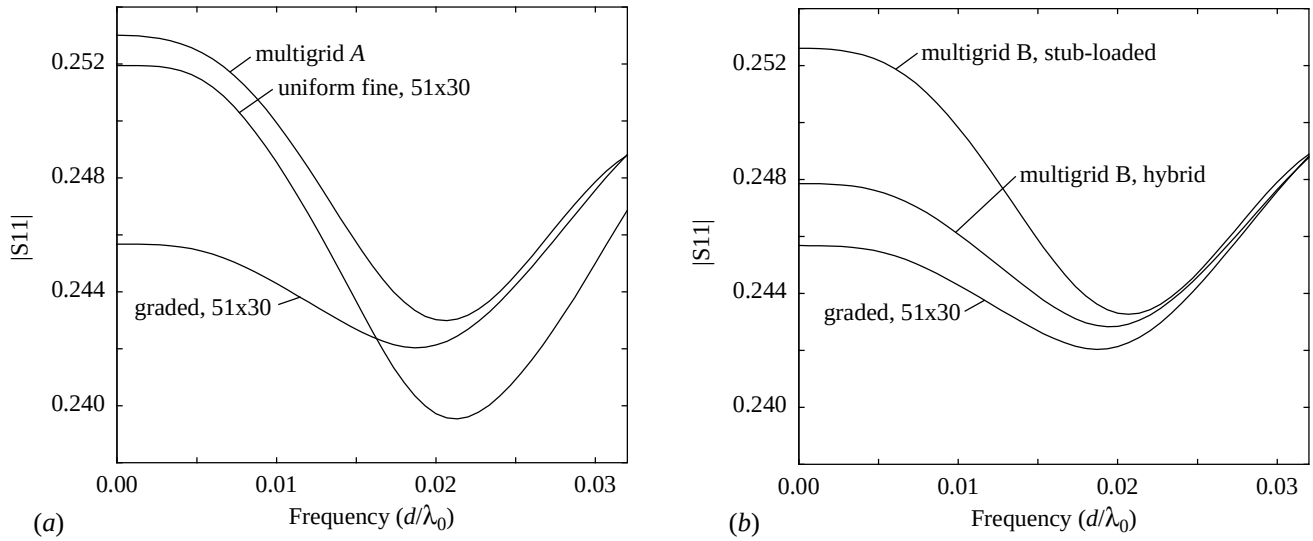

(*a*) (*b*)

Fig. 13 – Impedance step: comparison of graded mesh and multigrid schemes

Conclusions

Multigrid techniques provide an effective means of reducing the mesh resolution away from discontinuities. For the examples considered, method *B* gives better results than method *A*. However, for certain classes of problems, method *A* can give results more quickly without a significant reduction in accuracy. Graded meshes can be more accurate but require greater computer resources.

References

[1] P. B. Johns, "A symmetrical condensed node for the TLM method", *IEEE Trans. MTT*, vol. 35, no. 4, pp 370–377, Apr. 1987.

[2] R. Scaramuzza and A. J. Lowery, "Hybrid symmetrical condensed node for the TLM method", *Electronics Letters*, vol. 26, no. 23, pp 1947–1949, Nov. 1990.

[3] J. L. Herring and C. Christopoulos, "Multigrid TLM method for solving EM field problems", *Electronics Letters*, vol. 28, no. 20, pp 1794–1795, Sept. 1991.

[4] J. L. Herring and C. Christopoulos, "Solving electromagnetic field problems using a multiple grid transmission-line modeling method", *IEEE Trans. AP*, vol. 42, no. 12, pp 1654–1658, Dec. 1994.

[5] J. Wlodarczyk, "New multigrid interface for the TLM method", *Electronics Letters*, vol. 32, no. 12, pp 1111–1112, June 1996.

[6] M. I. Sobhy, M. H. Abd El-Azeem and K. W. Royer, "A new multi-grid 3-D TLM algorithm for simulation of microwave FSS", *IEEE MTT-S Symposium*, June 16-21 1996, San Francisco, CA, USA, pp 439–442.

[7] J. S. Nielsen and W. J. R. Hoefer, "Generalised dispersion analysis and spurious modes of 2-D TLM and 3-D TLM formulations", *IEEE Trans. MTT*, vol. 41, no. 8, pp 1375–1384.

[8] L. de Menezes and W. J. R. Hoefer, "Accuracy of TLM solutions of Maxwell's equations", *IEEE MTT-S Symposium*, June 16–21 1996, San Francisco, CA, USA, pp 1019–1022.

[9] L. de Menezes, C. Eswarappa and W. J. R. Hoefer, "A comparative study of dispersion errors and performance of absorbing boundary conditions in SCN-TLM and FDTD", *13th Annual Review of Progress in Applied Electromagnetics (ACES)*, 17–21 March 1997, Monterey, CA, USA, *this proceedings*.

[10] L. Cascio, G. Tardioli, T. Rozzi and W. J. R. Hoefer, "A quasi-static modification of TLM at knife edge and 90° wedge singularities", *IEEE MTT-S Symposium*, June 16–21 1996, San Francisco, CA, USA, pp 443–446.

[11] J. L. Herring and W. J. R. Hoefer, "Compensation of coarseness error in TLM modeling of microwave structures with the symmetrical condensed node", *IEEE MTT-S Symposium*, May 16–20 1995, Orlando, Florida, USA, pp 23–26.

[12] J. A. Porti, J. A. Morente, M. Khallad and A. Callego, "Comparison of thin-wire models for TLM method", *Electronics Letters*, vol. 28, pp 1910–1911.

[13] A. Mallik, D. P. Johns and A. J. Wlodarczyk, "TLM modelling of wires and slots", *10th International Zurich Symposium on Electromagnetic Compatibility*, 9–11 March 1993, pp 515–520.

[14] F. J. German, "Infinitesimally adjustable boundaries in symmetrical condensed node TLM simulations", *9th Annual Review of Progress in Applied Electromagnetics (ACES)*, 22–26 March 1993, Monterey, CA, USA, pp 482–490.

[15] Eswarappa, G. I. Costache and W. J. R. Hoefer, "Transmission line matrix modeling of dispersive wide-band absorbing boundaries with time-domain diakoptics for S-parameter extraction", *IEEE Trans. MTT*, vol. 38, no. 4, pp 379–386, Apr. 1990.

[16] M. Righi and W. J. R. Hoefer, "Efficient 3D-SCN-TLM diakoptics for waveguide components", *IEEE Trans. MTT*, vol. 42, no. 12, pp 2381–2385, Dec. 1994.

[17] J. L. Herring and W. J. R. Hoefer, "Improved excitation of 3D SCN TLM based on voltage sources," *IEEE MTT-S Symposium*, June 16–21 1996, San Francisco, CA, USA, pp 1019–1022.

[18] C. Eswarappa and W. J. R. Hoefer, "One-way equation absorbing boundary conditions for 3-D TLM analysis of planar and quasi-planar structures", *IEEE Trans. MTT*, vol. 42, no. 9, pp 1669–1677, Sept. 1994.

[19] C. Eswarappa and W. J. R. Hoefer, "Implementation of Berenger absorbing boundary conditions in TLM by interfacing FDTD perfectly matched layers", *Electronics Letters*, vol. 31, no. 15, pp 1264–1266, July 1995.

[20] N. Pena and M. M. Ney, "A new TLM node for Berenger's perfectly matched layer", *IEEE Microwave and Guided Wave Letters*, vol. 6, no. 11, pp 410–412, Nov. 1996.

[21] Eswrappa and W. J. R. Hoefer, "Diakoptics and wideband dispersive absorbing boundaries in the 3D TLM method with symmetrical condensed nodes", *IEICE Trans.*, vol. E 74, no. 5, pp 1242–1250, May 1991.

[22] K. Chang and P. J. Khan, "Equivalent circuit of a narrow axial strip in waveguide", *IEEE Trans. MTT*, vol. 24, no. 9, pp 611–615, Sept. 1976.

[23] N. H. L. Koster and R. H. Jansen, "The microstrip step discontinuity: a revised description", *IEEE Trans. MTT*, vol. 34, no. 2, pp 213–223, Feb. 1986.

Acknowledgments

This work has been funded by the Natural Sciences and Engineering Research Council of Canada, the Science Council of British Columbia, MPR Teltech Inc. of Burnaby, B.C., and the University of Victoria.